JAAS

PAPER

View Article Online
View Journal | View Issue

Cite this: *J. Anal. At. Spectrom.*, 2025, **40**, 2426

Influence of sample matrix and filter fixation on LIBS signal in analysis of algae on filter

Aleš Hrdlička, *[a] Jana Horská, [b] Jitka Hegrová, [c] Martina Bucková, [c] David Prochazka, [d] Jakub Buday, [d] Pavel Pořízka, [de] Viktor Kanický [a] and Jozef Kaiser [de]

This study first reveals the matrix effect mechanism of filter fixation on laser-induced breakdown spectroscopy (LIBS) quantitative analysis of algae, providing a methodological reference for *in situ* environmental detection. A collinear 1064 nm double pulse LIBS was used for analysis of green algae on a cellulose filter. Intensities of the contaminant elements Zn, Ni and those of some matrix lines of C I, Ca I, II, K I, Mg I, II, Mn I, II, Na I, H I, O I were measured and compared for various numbers of tape layers used for the filter fixation onto a microscope glass slide. This arrangement simulated surface modifications which can substantially lower the measured intensities. Maximum intensities were measured for 1 or 2 tape layers and lowest intensities for 6 layers for filters with contaminated algae; however, this intuitive result was not yielded for non-contaminated algae. It might indicate substantial changes of the filter properties and interaction with the laser beam at minimal changes of the analyte. This is crucial for quantitative analysis influenced not only by the sample fixation and surface quality but also by the composition of the filtered algae. The results were, to some extent, supported by principal component analysis, a shadowgraphic study of a single pulse microplasma shockwave, crater size and by simplified geometric and thermodynamic models. These were based on a spherical shape and full validity of the Boltzmann distribution respectively. The relatively small changes of the abovementioned parameters are in contrast to important changes of the lines intensities measured from the microplasma on the contaminated samples.

Received 13th June 2025
Accepted 25th July 2025

DOI: 10.1039/d5ja00236b

rsc.li/jaas

1. Introduction

Laser-Induced Breakdown Spectroscopy (LIBS) is a powerful analytical technique that utilizes laser pulses to vaporize and excite a small portion of a sample, generating a plasma plume. This plasma emits light, which is then analysed to determine the sample's elemental composition. LIBS offers several advantages, including real-time analysis, minimal sample preparation, short detection time, and applicability to a wide range of materials, including solids, liquids, and gases.[1–3] LIBS has found applications in various fields, including environmental monitoring,[4] industrial process control,[5] forensic analysis,[6] and archaeology.[7]

However, LIBS also has limitations. One of the key challenges is the quantitative analysis of elemental composition and the associated calibration.[8] LIBS requires high-energy laser pulses to create the plasma, which can be costly and may also damage delicate or small samples.[9] Another issue is matrix effects, where the presence of different elements and compounds in a sample can influence the intensity and accuracy of spectral lines, potentially leading to inaccuracies in quantitative analysis. Therefore, the interaction between the laser and the material, as well as sample fixation, plays a significant role in sample preparation. Compared to other methods, such as Inductively Coupled Plasma Mass Spectrometry (ICP-MS), LIBS eliminates the need for digestion. Among others, this capability is crucial in analysis of algae and other samples on filters.[10,11] While the most common method for processing algal samples for LIBS in the literature involves preparing pellets by grinding and pressing algae,[12] in our studies, filtration alone is used for sample preparation.[11,13]

Although laser ablation ICP-MS (LA-ICP-MS) coupled with triple-quadrupole or plasma-time-of-flight mass spectrometry (LA-ICP-TOFMS) are established techniques capable of performing very sensitive direct analysis of solid samples and offering high isotopic resolution, they involve significantly more complex and costly instrumentation, including the use of argon plasma and vacuum systems. In contrast, LIBS can be

[a]*Department of Chemistry, Faculty of Science, Masaryk University, Kotlářská 2, 611 37 Brno, Czech Republic. E-mail: ahrdlicka@chemi.muni.cz*

[b]*Department of Physics, Chemistry and Vocational Education, Faculty of Education, Masaryk University, Poříčí 7, 603 00 Brno, Czech Republic*

[c]*Transport Research Centre, Líšeňská 33a, 636 00 Brno, Czech Republic*

[d]*Central European Institute of Technology, Brno University of Technology (CEITEC BUT), Purkyňova 656/123, 612 00 Brno, Czech Republic*

[e]*Lightigo s.r.o., Renneská třída 329/13, 639 00 Brno, Czech Republic*

implemented with relatively compact, robust, and portable systems that do not require carrier gases, making it highly suitable for fieldwork and *in situ* analysis. Additionally, LIBS can simultaneously detect multiple elements, providing a rapid and comprehensive elemental profile of the algae. While it may not achieve the sensitivity of LA-ICP-TOFMS, LIBS provides a practical and efficient balance between speed, cost, and ease of use, especially for environmental applications and preliminary screening.[14]

These advantages make LIBS a particularly useful tool for analysing algae samples. Minimal sample preparation is required, allowing the sample to remain usable for further analysis, as the technique is minimally invasive. LIBS can directly analyse a filter with caught algae cells in real time. Further steps including a decomposition procedure to transform the algae sample into a liquid solution are omitted.[13] Furthermore, LIBS can detect multiple elements in a single measurement, which is valuable for monitoring levels of pollutants or heavy metals in algae, crucial for assessing environmental contamination and its impact on aquatic ecosystems. LIBS can also be used to analyse the biomass composition of algae, which is valuable for biofuel production.[15–17] Studies show that algae can accumulate trace metals through processes such as bioaccumulation and biosorption.[18]

Analytical methods, including LIBS, can be affected by various matrix effects. One such effect is the interaction of the laser beam with surfaces of varying hardness, which manifests as either an intense reflected shockwave and microplasma.[19] This interaction can be studied using, *e.g.*, shadowgraphy.[20] Among the optical methods, shadowgraphy is used to observe non-uniformities in transparent media, such as water or air, by observing changes in the refractive index of these media.[21–23] In the context of LIBS, shadowgraphy can be employed to observe the effects of different laser fluences.[24] For example, Gottlieb *et al.* used shadowgraphy to study the effect of particle grain sizes in different cement-based mixtures on laser-induced plasma evolution.[25]

During our previous analyses of algae-covered filters with LIBS, we observed changes in the microplasma size along with substantial variations in signal intensity. These occurred when the filter was not properly fixed to the base or when different groups of samples were ablated. This suggested that an underlying factor related to the material's interaction with the laser beam could be influencing the observed intensity changes. Consequently, we focused on the behaviour of spectra and microplasma images in relation to surface modification. Given the specificity of cellulose filter materials, surface changes modelling was achieved by applying multiple layers of double-adhesive tape to attach the filter to a microscope glass slide. Another factor examined was the presence or absence of contaminated algae on the filter surface. The influence of these parameters on signal intensity, sensitivity, and plasma properties is presented here. Line intensities, microplasma shockwave height, total emissivity, crater depths, Principal Component Analysis (PCA), and simple geometrical and thermodynamical models were applied to isolate specific contributions to the measured intensity changes.

2. Experimental

2.1 Sample preparation

The ecotoxicological tests were carried out with the green alga *Desmodesmus subspicatus* (BRINKMANN 1953/SAG 86,81). Green algae are photosynthetic aquatic eukaryotic organisms that have a high capacity for biosorption of heavy metals. The high sorption capacity of algae is due to the composition of their cell wall. *Desmodesmus subspicatus* is a unicellular freshwater green alga whose cell wall contains polysaccharides (mainly cellulose), proteins and lipids with various functional groups, such as carboxyl, hydroxyl and sulfhydryl, which are responsible for the high sorption capacity of metal ions.[26] The algae were taken from The Institute of Botany of the Czech Academy of Science, Department of Experimental Garden and Collection of Aquatic and Wetland Plants (CCALA) Třeboň, Czechia.

Green alga *Desmodesmus subspicatus* was left in a solution with Zn and Ni concentration of 0.3 mg L^{-1} each and after the contamination period was filtered through a nitrocellulose filter (type: 0.45 μm MCE membrane, 47 mm diameter, nonsterile, hydrophilic, Merck Millipore Ltd). Ecotoxicological tests were carried out in accordance with EN ISO 8692 (ISO 2012). The analysis was carried out in 125 mL of Erlenmeyer flasks containing 60 mL of the analysed solution. The solutions of the tested metals were prepared in the growth medium (the composition is described in ISO). A control group contained only the growth medium with the addition of algae. The samples of control group and tested samples (samples with added metals) were then incubated for 72 hours in the thermostat TS 606 CZ/2-Var (WTW, Czech Republic) at the temperature of (23 ± 2) °C with constant shaking on the orbital shaker at 100 rpm (IKA KS260 basic, Germany) and constant illumination ranging from 68 to 94 μmol photons per m^2 per s. Control samples contain algae in growth medium, tested samples contain algae in growth medium with addition of toxic metals. Afterwards, it was dried and the filter with the contaminated algae was fixed with a thin double adhesive tape to a microscope slide that was attached onto a movable xyz LIBS platform. The surface concentrations on the filter calculated from reference ICP-MS (8800 ICP-QQQ Agilent Technologies) analysis were 25 and 64 ng cm^{-2} for Ni and Zn respectively.

2.2 Instrumentation of inductively coupled plasma mass spectrometry

The content of selected elements was determined with the use of ICP-MS/MS (Agilent, Japan). Selected elements Zn and Ni were analysed using a collision reaction cell, masses ^{60}Ni, ^{66}Zn using He collision gas (4 mL min^{-1}) measured on mass in single quadrupole mode. Integration time per isotope was 0.3 s, carrier gas flow rate 1.07 L min^{-1}, forwarded RF power was 1550 W. Calibration solutions were prepared from the stock solutions of single-element standards with a concentration of 1 g L^{-1} (Analytika, CZ), the same standards were used for algae contamination. The internal standard of 10 μg L^{-1} was prepared from the Agilent 10 mg L^{-1} stock solution (internal standard mix).

2.3 Instrumentation of double pulse LIBS

A doubled 1064 nm Nd:YAG laser for collinear double pulse 1064/1064 nm LIBS for signal enhancement was used. The detection basis for gate delay (GD) was the launch of the 2nd pulse. A Czerny–Turner 0.5 m spectrometer Andor 500 with a sCMOS detector for detection of Zn and Ni lines and an echelle spectrometer Catalina Scientific (range 200–1000 nm) with an EMCCD detector for overview spectra acquisition were employed. The sample was placed in a LIBS chamber and the surface was rinsed with Ar (1 L min^{-1}) as another source of signal enhancement. Each pulse was fired onto a fresh surface so that it did not make a hole in the filter. A matrix of 5 × 5 craters was produced, signal from each 5 consecutive pulses was integrated on a chip so that from 25 pulses a set of 5 intensities was obtained. The instrumentation was the same as in the previous study[13] as well as the 1st pulse energy of 23 mJ, 2nd pulse 30 mJ, interpulse delay of 0.04 μs and GD = 0.7 μs as optimal values.

2.4 Sample fixation for LIBS

The surface modification was modelled with various numbers of double adhesive tape layers between the filter and the glass slide (Fig. 1). On the microscope glass slide 1, 2, 3, 4 or 6 double adhesive tape slices were glued over each other (Fig. 1). The filter sample was finally glued on the top tape layer. The filter area with algae contaminated with Zn and Ni was named as "sample", the pure filter rim of this "sample" out of the filtration area was named as "sample blank", the area of another piece of the filter with non-contaminated algae as "control" and its filter rim as "control blank". These four parts were analyzed with LIBS.

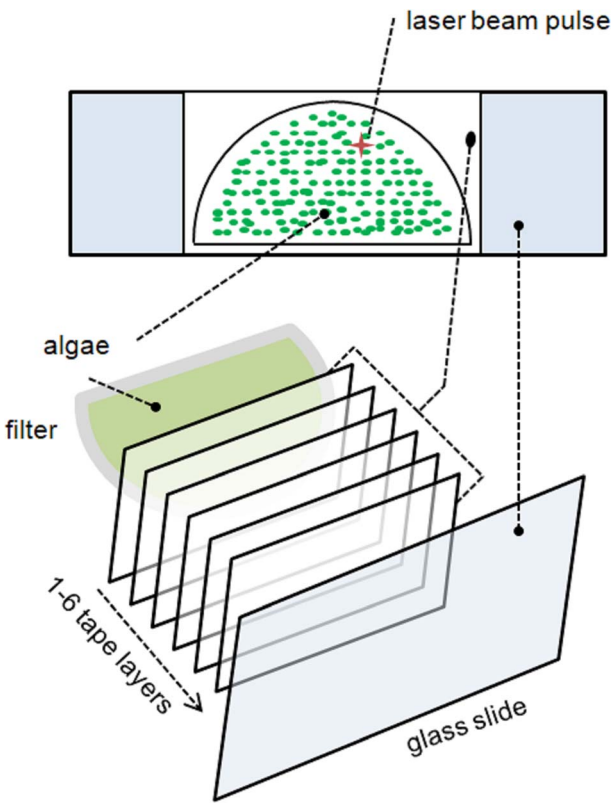

Fig. 1 Fixation of the filter using 1–6 tape layers.

2.5 Instrumentation with shadowgraphy and single pulse LIBS

An expanded diode pumped continuous laser of 532 nm passing through the region of the plasma plume and captured by an ICCD camera was used. The camera was set to acquire images 2 μs after firing the ablation pulse, and the duration of the exposure was 100 ns. The radiation for LIBS was collected at 0.7 μs after the ablation pulse for 15 μs. The ablation laser (1064 nm, 23 mJ, duration ~ 10 ns, beam diameter 6 mm, operating at 50 Hz) was focused on the sample with a fused silica triplet (focal length 50 mm) into a 30 μm spot, so that the LIBS conditions were set as similar as possible to the DP LIBS variant. Radiation of the plasma was collected using a collimator (38.5 mm focal length) and an optical fiber with a 400 μm core diameter onto an echelle spectrometer (resolving power $\lambda/\Delta\lambda = 5000$) equipped with an ICCD camera.

Shadowgraphy detects the second derivation of the refractive index. Therefore, in combination with LIBS, it is used to detect and observe generated shock waves, containing information about their size, shape, or velocity. Its velocity or size is proportional to its initial energy, which also reflects the properties and influence of the ablated sample. An example of such an image is in Fig. 2. This study did not enable identical conditions as the shadowgraphic set-up was in a different laboratory equipped with a SP LIBS. However, the ablation laser was operated 1064 nm at the same pulse energy of 23 mJ as the ablation pulse in DP LIBS. Also the filter was always the same as in case of DP LIBS and the echelle SP LIBS spectrum was recorded simultaneously with the shadowgraphic image.

The used shadowgraphic parameters for an objective study was the shockwave height.

2.6 Instrumentation for measurement of crater depths and profiles

Shapes and sizes of ablation craters were examined with optical microscopes 4K Keyence VHX-7000 (Belgium) and Euromex T-MS-100 BioBlue (Microscopes Holland).

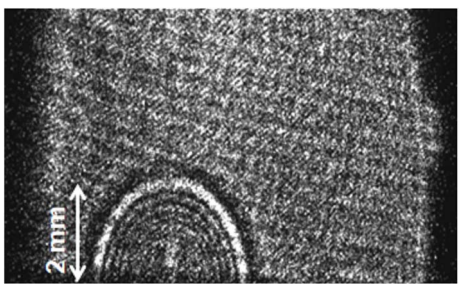

Fig. 2 Shadowgraphic image of the single pulse microplasma on the filter.

3. Results and discussion

3.1 Semiquantitative study of contaminant, minor and matrix elements

The analytes Zn, Ni were first investigated in terms of their line intensities. As the DP LIBS instrumentation was the same as in the previous study[13] the experimental conditions were kept identical (see Experimental part). The results for DP LIBS with the Czerny–Turner spectrometer can be seen in Fig. 3 for the intensities corresponding to the areas of the Zn or Ni peaks. The SP LIBS with shadowgraphy was not equipped with a sensitive spectrometer to detect Zn and Ni emission. An example of the spectrum has been already shown.[13] The control and blank samples showed only close to zero intensities of Zn and Ni. The intensities of Zn and Ni on the "sample" are 5 accumulations without the background (area) which was subtracted aside the peak. "Blank" and "control" intensities were yielded by the same way. Considering the concept of 3-sigma Limit of Detection (LOD), all the depicted points except Zn at 6 layers were above it and the yielded shape of the trend is statistically significant. The last points for 6 tape layers are, however, close to LOD. In the whole article, the used error bars were 95% confidence intervals from five integrated spectra, not standard deviations. Each integrated spectrum was composed from 5 single shot spectra, so that 25 spectra were used for one point. A statistical evaluation by Dean and Dixon[27] was applied. This is fully acceptable with regard to the required precision of the contamination studies.

Although this is a primary semiquantitative study without more points in a calibration curve the LODs can be easily calculated by the 3-sigma rule: 3 standard deviations of the signal from the blank filter (in Fig. 3, "blank"), without algae divided by the slope (signal of the analyte from the contaminated filter divided by the reference concentration 64 for Zn and 25 ng cm^{-2} for Ni from ICP-MS). The LODs for 1–6 tapes are (ng cm^{-2}) – Zn: 14, 15, 15, 28, 83; Ni: 4.7, 3.7, 9.7, 7.2, 17.

Next part was dedicated to the response of other lines representing elements in the solution or in the filter material. To record broadband spectra with a full portfolio of the sufficiently contained (*i.e.* above LOD under any conditions) elements, an echelle spectrometer was employed parallel with the CT one in the DP LIBS and solo in the SP LIBS with shadowgraphy.

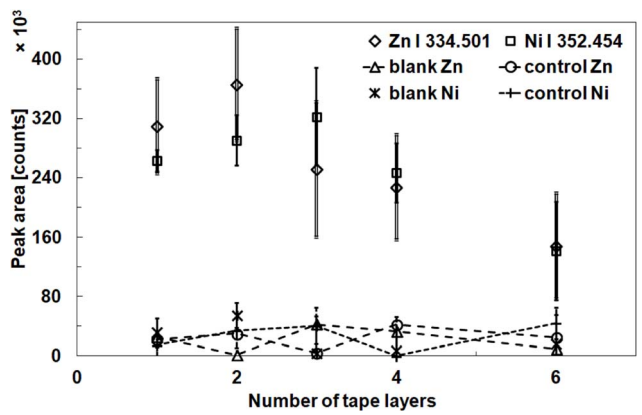

Fig. 3 Response of the zinc and nickel lines as areas under curves on the number of used tape layers. Error bars are 95% confidence intervals, not standard deviation. Measured with a Czerny–Turner (CT) spectrometer in a double pulse arrangement.

The behaviour of some matrix lines is presented in Fig. 4. There are selected lines with an excitation energy which is low (K I, Mn I), medium (Mg I) and high (C I). Also, there are ionic lines with a high sum of the ionization and excitation energies (Mn II, Mg II). This part discusses differences between SP and DP LIBS and among the lines in response on the number of tape layers. As the dependences are not normalized original intensities can also be compared. DP LIBS intensities are more stable than the SP LIBS ones and control samples are also more stable in the response on the tape layers than the samples with contamination. This is best valid for C I in Fig. 4a and b which is also the most abundant matrix element. Although the dependences for SP and DP LIBS are similar the differences between the samples and controls cannot be considered as identical, mainly for the Mg I line. Except for possible matrix effects, the main contributor is probably a distortion by reading of low intensities of Mg I and Mn I lines from the SP LIBS. Otherwise, it does not seem that the shapes of the dependences are dependent on the line excitation energy. The investigated analytes Zn and Ni follow the same behaviour (Fig. 3). The main responsible source of the observed changes is probably the surface modification by the tape layers. Although there are also the analyte atoms in the samples, their influence on the more easily excitable and ionisable alkali atoms seems to be improbable in the laser microplasma. The relations among the particular elements will be shown and discussed later based on their lines intensities, excitation and ionization energies.

Each tape layer adds 0.084 mm of thickness. This fact did not influence the laser beam focusing because each ablation area on the slide with the tapes and the filter was focused individually. Again, the maximum intensity and the best signal to noise ratio of the matrix lines is for 1–2 tape layers for samples while the controls can have the maximum shifted to another number of layers. The curves for controls are moreover less regular than the samples ones. It indicates that the 2 layers somehow positively modify the filter–beam interaction. This phenomenon prevails over the negative effect observed for more than 2 layers.

Next step was a preliminary quantification study from affordable data. The Zn, Ni contaminants had only one concentration in the samples. Blanks and controls were not zero according to ICP-MS results, however, nearly on the noise level according to LIBS results. However, some matrix elements provided usable intensities (Fig. 4) so that 3 concentrations were available (samples, controls, blanks). Their intensities could be compared with ICP-MS concentrations and plotted for 1–6 tape layers in Fig. 5 from more intensive DP LIBS echelle spectra in about 200–1000 nm range. The left column of Fig. 5a, c, e, g and i represents samples, controls and blanks from the samples with Zn, Ni while the right column (b, d, f, h and j) contains blanks from the controls (also with algae but without Zn, Ni). It is evident that the controls provide higher intensities than the samples. The influence of the tape layers is not monotonous for the controls but it is already better presented in Fig. 4. A more detailed study of the matrix effects follows in next

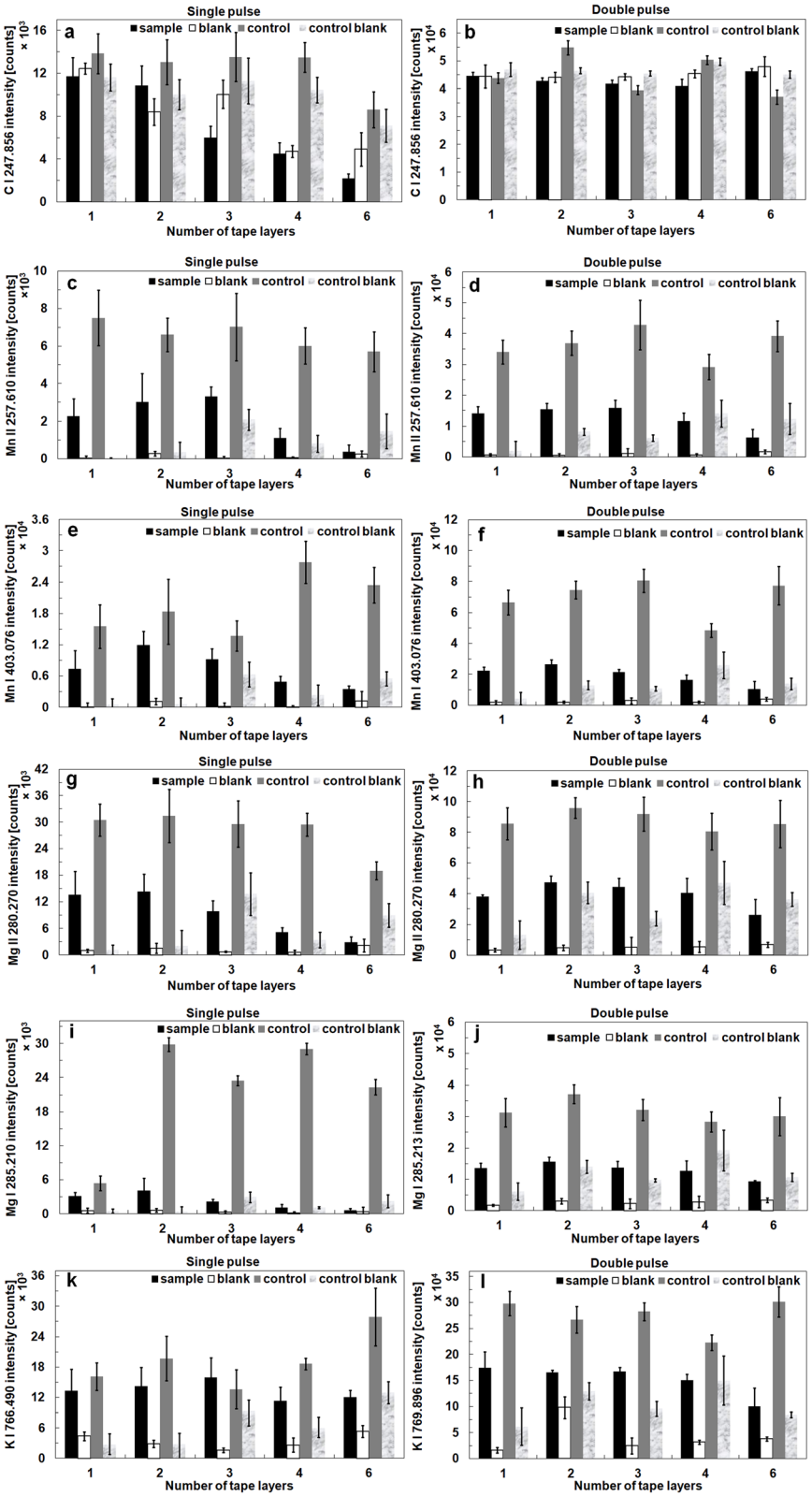

Fig. 4 Response of some lines of matrix elements (measured with echelle) on the number of used tape layers from single pulse (a, c, e, g, i and k) and double pulse LIBS (b, d, f, h, j and l).

two chapters. The first one is a multielemental calibration approach to get around the lack of samples with different concentrations.

Such an approach tests a broadband linearity and matrix effects. There are only a few concentrations: for sample, blank and control sample of the elements coming from the solution and the

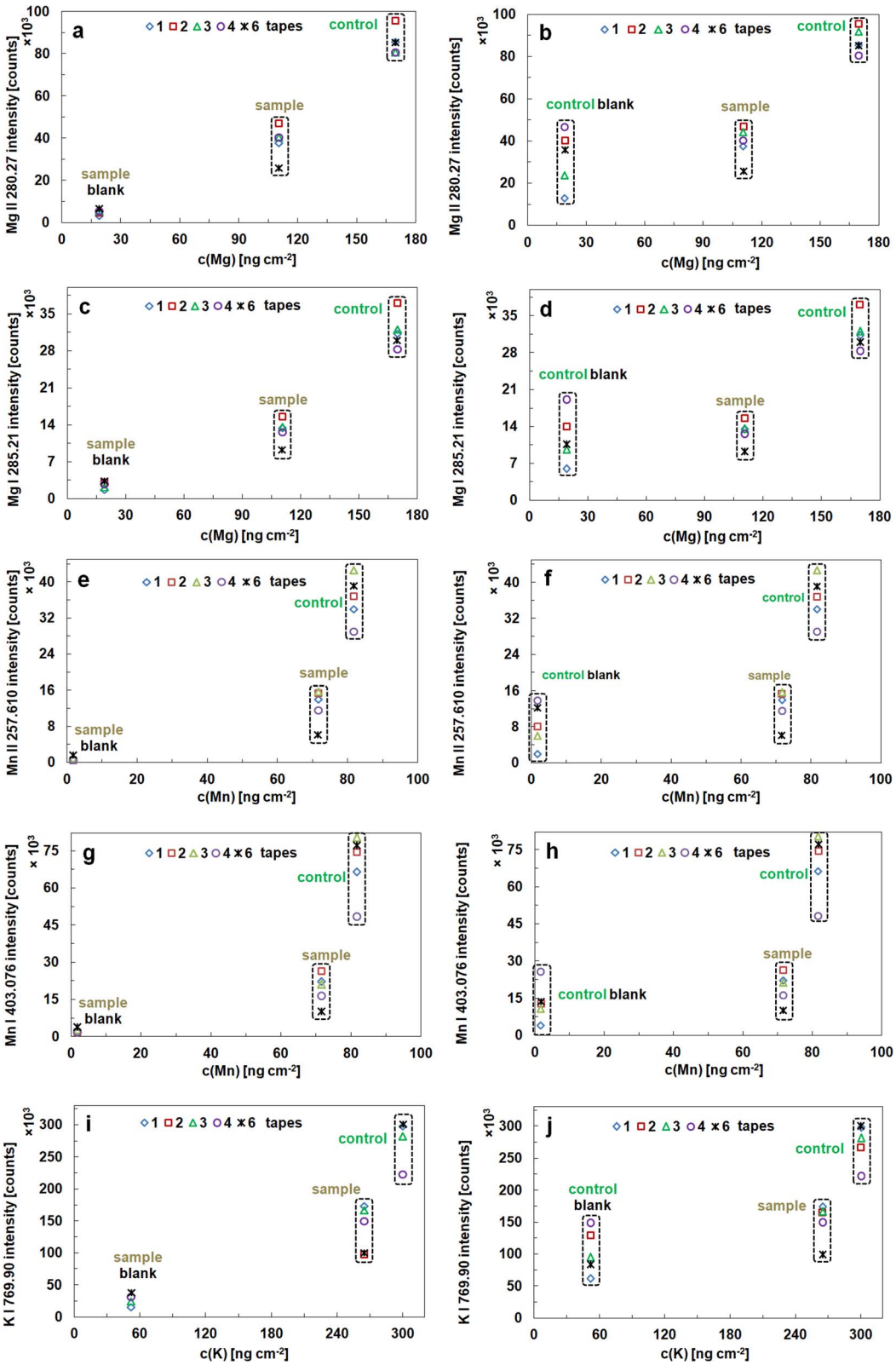

Fig. 5 Intensities of the selected element lines (from echelle double pulse) as a function of elements contents by ICP-MS for the samples with Zn and Ni as analytes and control or blank filters without added Zn, Ni. Sample blank is shown in the left column (a, c, e, g and i), control blank in the right column (b, d, f, h and j). Number of tape layers is marked as 1–6.

filter body. The measured intensity I of the particular element n was first normalized to its maximum I_{max} (we get I_n) and secondly all the intensities of all the elements were normalized to the global maximum element concentration c_K which was 300 ng cm^{-2} of potassium (we get I_N). The particular elements concentrations c_n and c_K are also taken from ICP-MS analyses:

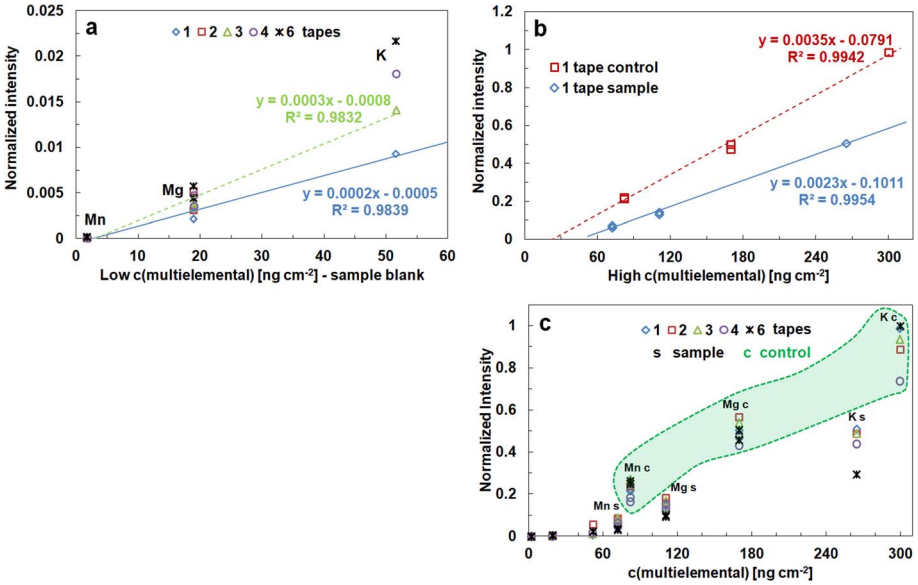

Fig. 6 Multielemental pseudocalibration dependences (from echelle double pulse) of some matrix elements from ICP-MS analyses. Low concentrations are plotted in (a), high concentrations in (b) and all concentrations are depicted in (c) with a green enclosure for the control samples.

$$I_n = I/I_{max} \quad (1)$$

$$I_N = I_n c_n / c_K \quad (2)$$

By these operations the points in the following pseudocalibration dependences show linearity across various lines and possible changes of the slope (Fig. 6). The presented results are from DP LIBS providing higher intensities than SP LIBS.

The normalized calibration dependences can be divided into two separate parts (Fig. 6a and b). They are both fairly linear, yet from 3 points (Fig. 6a and b). The first one for lower concentrations close to the LOD indicates 11 times lower slope than for higher concentrations over 60 ng cm^{-2}. Another result confirms the overall observation that control samples provide generally higher signal by a factor of 1.5. It means that the filter material properties are changed by application of a non-contaminated solution with algae. All the points are depicted in Fig. 6c with a green enclosure of the control samples.

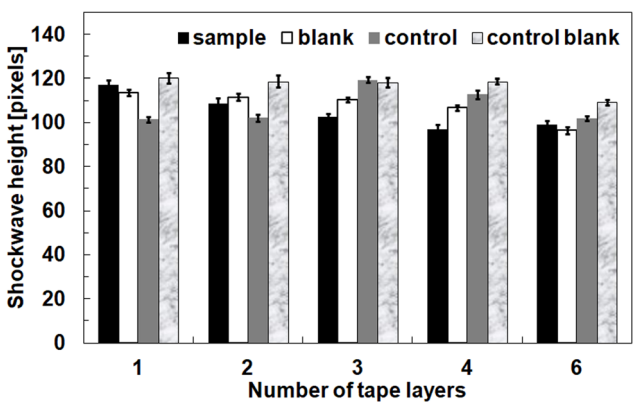

Fig. 7 Single pulse shockwave heights.

Further study is focused on the plasma body itself.

3.2 Shadowgraphic study

The height of the shockwave (Fig. 7) was measured in pixels from the dark base to the upper end of the brightest ring (Fig. 2) by a visual inspection using a PC mouse in ImageJ-win32 software. The presented numbers are averages from 25 laser pulses. Similarly to the DP LIBS results there is a direct decrease with the number of tape layers for the samples while the controls are less pronounced. The observed decreases are lower than those of the spectral lines and cannot themselves fully explain their deeper drop in Fig. 3 and 4. However, a stronger effect of the layers on the samples than on the controls was once more confirmed.

Changes of the total emissivity can be used for comparison of both SP and DP LIBS spectra behaviour (Fig. 8). It is clearly distinguishable that the DP LIBS method provides more stable spectra by comparison of the error bars and a relative stability over the tape layers. Once more the biggest decrease was observed for the samples at SP LIBS.

3.3 Measurement of crater depths and areas

Next part was checking depths and areas of ablation craters using optical microscopy but no systematic change was found on individual craters. The variability from pulse to pulse is quite large but some differences are well provable if all the 25 crater depths for one set ablated on the particular tape base are averaged. The cellulose is a difficult material for craters profiling. The shape was similar to a hyperboloid with not very well defined bottom or surface diameter of about 0.17–0.19 mm. The dependence of the DP-LIBS crater depth on the number of tape layers is plotted in Fig. 9. It confirms the enhanced crater depth at the controls and gives reason for the observed higher

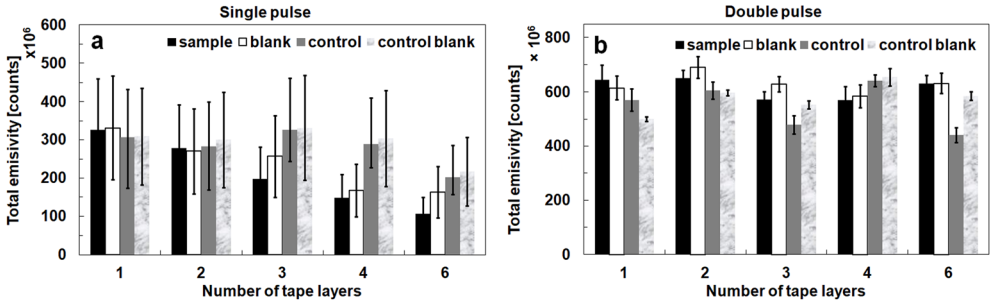

Fig. 8 Total emissivity as a function of the number of used tape layers from single pulse (a) and double pulse (b) LIBS.

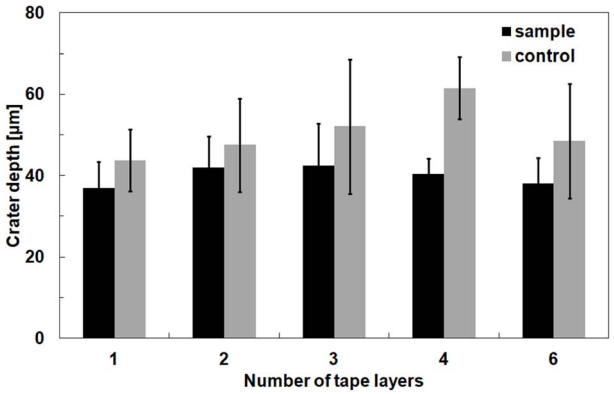

Fig. 9 Crater depths as a function of the number of used tape layers.

matrix lines intensities than at the contaminated samples. The beam affected crater area is also systematically larger on the controls as measured by the microscope. Specifically, it is the ratio of control-to-sample crater area of 1.7 for DP-LIBS and 1.2 for SP-LIBS. Also the relative area uncertainty (at probability 95%) is 27% for samples, 15% for controls from DP-LIBS and 54% for samples, 29% for controls from SP-LIBS. It is not clear how are the matrix and the analyte elements distributed within the filter volume but the crater dimensions changes give reason for the observed increase of the lines intensities. According to the green crater orifice and white interior the cells are situated at the surface. Apparently greener and darker control filter surface with much higher number of living green algae cells, not poisoned by Zn, Ni, may better absorb the laser beam energy. A reflectance spectrum of chlorophylls shows an infrared plateau including 1064 nm. Depending on the particular dye 39–52% of the radiation is reflected.[28] It is highly probable that less coloured or white part of the filter reflects more laser radiation. The ablation threshold may be lower and the ablated area larger on the greener control samples than on the samples. The penetration depth of 1064 nm laser in cellulose is about 0.1 mm, and 6 tape layers (0.504 mm) may cause energy attenuation. Mechanical tests with the filters consisted only of a filter bending to see if a crack damage appears. However, nothing was observed for both the sample and control filters. The craters from controls and samples are compared in Fig. 10. The sample crater snapshot with its neighbourhood is merged in the controls area. It is focused onto the surface and the craters insides are thus defocused. The colour is not true from the illumination but the control surface is more colour covered than the sample one with more bulging filter contours.

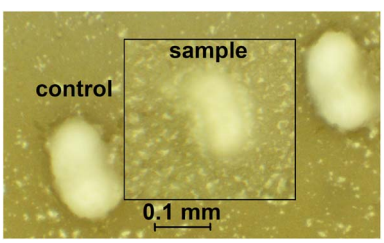

Fig. 10 A detail of DP-LIBS ablation craters on control and sample filter. A sample cutout is merged with the control snapshot.

3.4 Investigation using principal component analysis of the spectra

To recover possible relations among samples Principal Component Analysis (PCA) was applied to whole echelle spectra. There is, in principle of PCA, no clear answer concerning the reasons for the relationship. However, the visualisation can be helpful and sufficient at the searching. There is generally not too much separation in the PC space except PC1–PC2 for SP LIBS (Fig. 11). The PCA scores (Fig. 11a) depict a separation of the control samples from each other by the number of the layers and from the samples with Zn and Ni. On the contrary, the Zn, Ni samples are not separated by the tape layers. The loadings (Fig. 11b) show 4 PC which might also here visualize also the rest of variability in contrast to the scores (no separation in a higher PC space). Maximum variability falls here on most intense lines and looks like a spectrum. It corresponds with the different contents of the elements and intensities of their lines (Fig. 4–6). Among them, the largest difference is in magnesium and potassium contents between the samples and the controls. Despite these differences their lines do not cover maximum variability (Fig. 11b). It is also possible that samples with Zn, Ni would also be separated by the number of tape layers if their lines intensities (matrix lines visible in the echelle broadband spectra) were as strong as those of the controls. The rule of the higher variability on the more intensive lines is confirmed by *e.g.* oxygen lines around 777 nm (Fig. 11b). This element is in the ambient air and in the filter matrix together

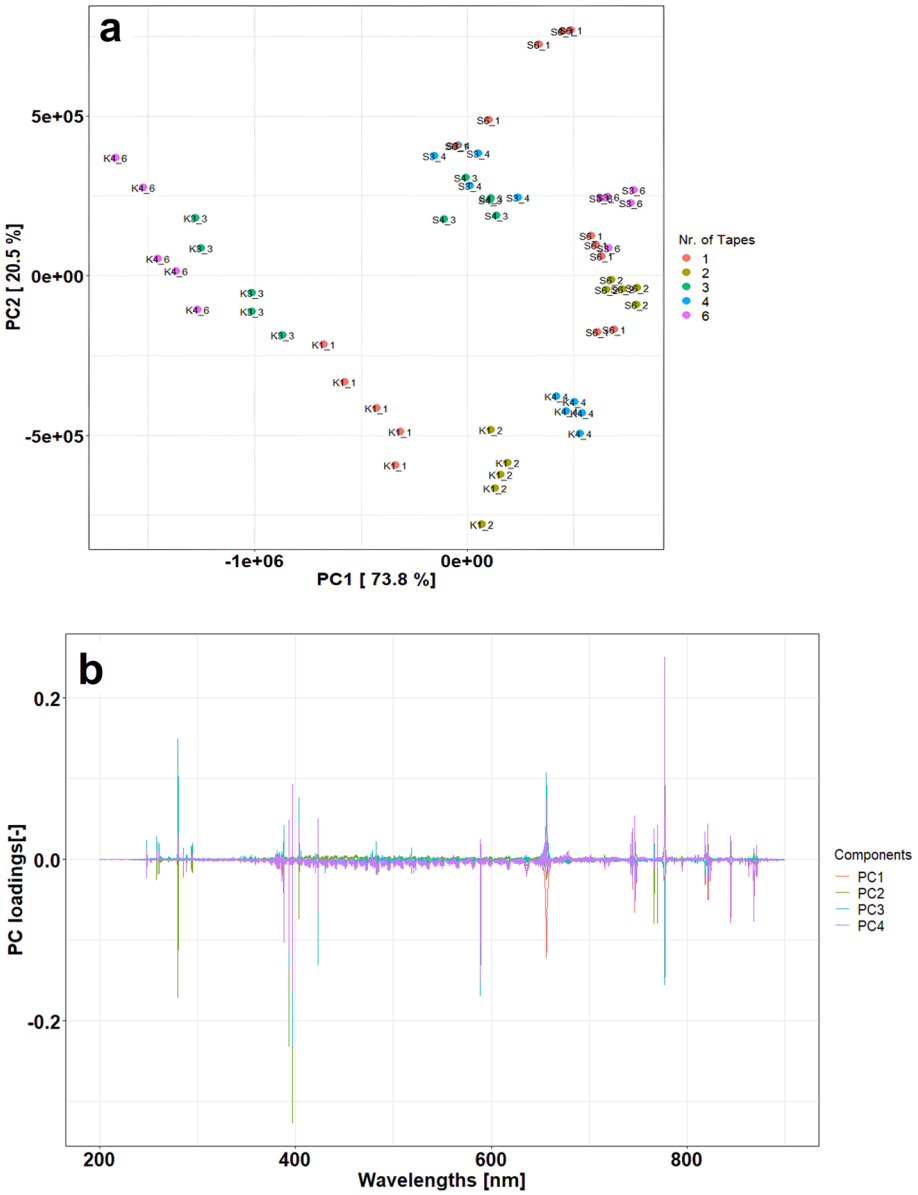

Fig. 11 Score plot (a) and loadings (b) of the principal components analysis and samples separation yielded from SP-LIBS spectra.

with carbon and hydrogen. On the contrary, the line of C I 247.856 nm comes mainly from the filter material. It is thus clear that the sources of the variability are the lines intensities, not the origin of their parent elements (pure filter body, algae solution, ambient atmosphere).

As a result, the control samples really show a different spectral response from the Zn, Ni ones and the algae solution substantially changes the mechanical properties of the filter and response on the laser beam. PCA loadings from DP LIBS do not separate the samples and are not presented. The reheating plasma at DP LIBS apparently diminishes the influence of the sample matrix (*e.g.* Fig. 8). The relation between the ablation laser beam and the filter is evidentially damped down with the 2nd pulse. To separate contaminated and non-contaminated samples the practical use of PCA is limited by the SP LIBS only. On the other hand, the DP LIBS system with the Cz-T spectrometer can directly detect the contaminant elements which is not possible with the SP LIBS connected with the echelle spectrometer only.

3.5 Geometric and thermodynamic considerations of the laser-induced plasma

Another part of the investigation is a comparison of possible geometrical and thermodynamic changes of the plasma. Considering a special case that the intensity changes happen only because of a lowering or enhancing the plasma size without a change of the plasma surface radiation per area unit it can be simply derived at keeping the observation angle constant that the squared (surface $\sim r^2$) ratio of the plasma radii $(r_6/r_1)^2$ is directly proportional to the measured intensities ratio I_6/I_1 (Fig. 12).

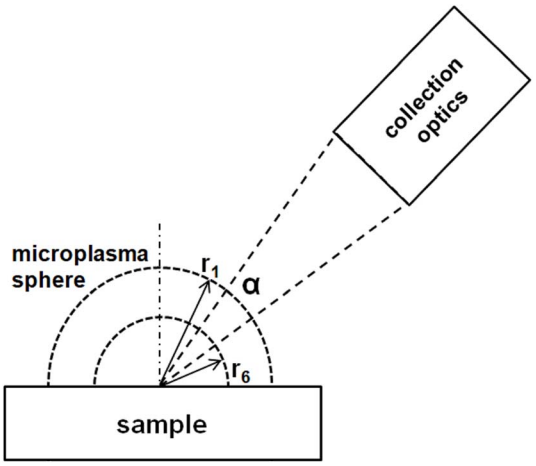

Fig. 12 Geometric spherical model of the microplasma and collection of the radiation.

Here the index 6 means 6 tape layers and 1 one layer. Taking the results from the plasma shadowgraphy we obtain the squared ratio of the shockwave heights to be 0.715, which is the values for SP LIBS because DP LIBS is not connected with shadowgraphy. By comparing the intensities of selected lines, the highest density of the points in the graph is really around the geometrical ratio (Fig. 13a, dashed line). It cannot be statistically proven but it can be stated that the microplasma size and the suggested geometrical aspect is really a key factor responsible for the majority of the measured intensity changes.

The thermodynamic considerations are strongly influenced by practical aspects of the LIBS experiment. It is especially a long integration time (gate width) of the detector and a lack of thermometric species. Some pairs of Mn II or Mg I lines with sufficiently different upper energy levels are usable for plasma temperature calculation but the content of these elements is inferior in some cases to use a less intensive line from the pair. Nevertheless, departures from Local Thermodynamic Equilibrium (LTE) can be relatively observed as follows. Let us consider a change of the plasma temperature from T_1 with one used tape layer to T_6 with six tape layers. By setting for the intensities ratio I_1/I_6 the ideal Boltzmann distribution (the whole relation for the intensity with g, A and other constants is not necessary – they are eliminated in the fraction) and logarithm the relation we obtain:

$$\ln(Z_1(T_1)I_1/Z_6(T_6)I_6) = E/k(T_1 - T_6)/(T_1T_6) \quad (3)$$

where $Z(T)$ is the partition function at an excitation temperature T, k is the Boltzmann constant and E is the energy of the upper level of the transition or the sum of the ionization and excitation energy and eventually also of a correction factor for ionic lines in Saha equation.[29] By dividing the eqn (3) by E we simply obtain for small changes of T:

$$\ln(Z_1I_1/Z_6I_6)/E = (T_1 - T_6)/(kT_1T_6) \approx \text{const for } T_6 \to T_1 \quad (4)$$

A possible effect of temperature changes on $Z(T)$ was estimated using a NIST calculator of partition function.[30] As a reference temperature 1 eV was taken and changes of the left side of (4) were calculated for ±0.1 and 0.2 eV. It is clear that in a very ideal case without departures from LTE, Boltzmann distribution, self-absorption and experimental factors, the points in Fig. 13b should be ordered in a horizontal line. As expected, this is not the case but lowest dispersion of the points in Fig. 13 is for $T_1 = T_6$ in case of SP LIBS "sample", "blank" and

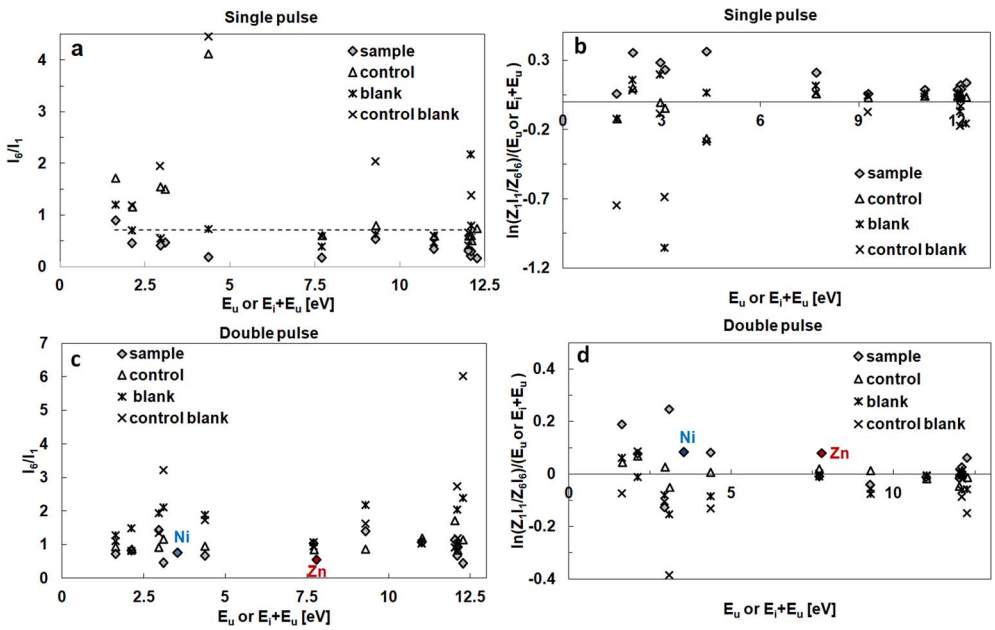

Fig. 13 Thermodynamic aspects of the lines ratios. Dashed line in (a) and (c) are theoretical intensities ratios from geometric changes of the plasma size (Fig. 12). Points in (b) and (d) should ideally be in one horizontal line (not necessarily zero on the vertical axis).

DP LIBS "sample", "control" and "control blank". The points of SP LIBS "control" show minimum dispersion for $T_1 = 1$, $T_6 = 0.9$ eV and also for the pair of $T_1 = 1.2$, $T_6 = 1.1$ eV while "control blank" and DP LIBS "blank" show once more lowest dispersion for $T_1 = 1$, $T_6 = 0.9$ eV. The lack of thermometric species and their sufficiently intensive lines does not allow for more precise determination of T or relative changes of T. Nevertheless, the above considerations indicate possible temperature changes within 10%. In any case, the higher the upper line energy (including ionization energy) the lower the deviation from the common horizontal line (Fig. 13b and d). The hard lines requiring a high excitation energy or sum of the excitation and ionization energy, which are of C I, N I, H I, O I, Ca II, Mn II, Mg II, are better linearly organized than the soft ones of Mg I, Mn I, K I, Na I, Ca I. The result is independent of the SP or DP LIBS arrangement, only DP LIBS is more stable and shows lower deviations from the line (the DP vertical axis is more magnified). By setting the lines of Zn, Ni contaminants into the Fig. 13b we can see that they are well depicted among the other lines although they are measured with the Czerny–Turner spectrometer parallelly with the echelle one providing the broadband spectra with all the other lines. The lines of the Zn and Ni contaminants are fully incorporated in the set of the other lines. No deviation is observed there and thus no special thermodynamic behaviour is supposed. The spectrometer choice is not relevant here. These observations are in a good agreement with the former work.[29] A possible departure from LTE has a bigger effect on the lower excitation energies than on the higher ones. The energy gap between a fundamental and a low energy excited state (*e.g.* Na I, K I, Ca I, Mn I) is more susceptible to disturbances and $Z(T)$ of that species changes significantly. However, the observed departures do not negatively influence the multielemental calibration lines and possibilities of successful quantification.

4. Conclusions

A successful detection of Ni and Zn in algae on the filter with DP-LIBS was demonstrated without the need of a time-consuming decomposition and consequent ICP-MS analysis of the solution. Semiquantitative determination of the metals both minor and more concentrated is currently possible. The LIBS analysis is applicable in the order of tenths of mg L^{-1} of the Zn and Ni contaminants in the solution with the *Desmodesmus subspicatus* freshwater green alga. The LOD of the measured metals is at the level of about 10 ng cm^{-2} for the DP system provided that the sample filter fixation to the base glass is correct and optimum conditions are maintained. Sensitivity to the sample fixation and matrix effects is proven. To ensure a maximum LIBS signal, the optimum fixation of the filter to the base glass for LIBS is the use of one or two layers of a double side adhesive tape between the filter and a glass. The main matrix effect is apparently a different interaction of the laser plume with the Zn, Ni contaminated and not contaminated filter material. Based on the greener and darker surface of the control non-contaminated filters it can be explained by lower ablation threshold than on the contaminated lighter pale green surface with many decolorized dead algae cells. This is supported by deeper and larger ablation craters on the control filters. The used Gaussian beam can more participate in the ablation with its profile wings. Without the contamination, the lines intensities substantially increase. This effect, however, goes around the determination of Zn, Ni because they are absent in the pure algae. Possible recommendation may consist in keeping stable conditions, mainly careful bonding of the filter. Concerning the lasers as another source of instabilities the DP 1064 nm system is relatively much more stable and sensitive than SP one. The analyte lines are more sensitive to the bonding of the filter than the other lines belonging to the elements naturally present in the algae solution or filter body. With a very weak bonding effect or even without it, the C I 247.856 nm matrix line and the electron number density are found. A certain effect at the level of units of per cents is measured for the size of the plasma shockwave. This mechanical aspect is an important contribution to the observed matrix effects.

The degree of the experimental departures of the lines from the thermodynamic equilibrium agree with theoretical presumptions[29] and do not negatively influence quantification of the matrix elements. A potentially remaining diagnostic method would be spatially resolved spectroscopy of the microplasma plume to yield distribution of the radiating atoms and ions of the analytes. However, this method is currently not feasible with accessible technical equipment.

Data availability

Data for this article, including raw spectra are available at Zenodo at **https://doi.org/10.5281/zenodo.15650002**.

Conflicts of interest

The authors declare that they have no known competing financial interests or personal relationships that could have appeared to influence the work reported in this paper.

Acknowledgements

Jiří Marenczok from Keyence International is deeply acknowledged for the crater profiles measurements using the Keyence VHX-700 microscope at the laboratory of Brno Campus Science Park. This work was supported by the Ministry of Transport of the Czech Republic within the programme of long-term conceptual development of research institutions. AH, and VK acknowledge the project MUNI/A/1691/2024. PP and JK acknowledge the support of the Czech Grant Agency (GACR Standard project, no. 22-27580S). JK acknowledge the support of the Brno University of Technology (FSI-S-23-8389).

References

1 R. Noll, *Laser-Induced Breakdown Spectroscopy - Fundamentals and Applications*, Springer, Berlin, Heidelberg, 2012.

2 S. Musazzi and U. Perini, *Laser-Induced Breakdown Spectroscopy: Theory and Applications*, Springer, Berlin, Heidelberg, 2014, DOI: 10.1007/978-3-642-45085-3.
3 G. Galbács, *Laser-Induced Breakdown Spectroscopy in Biological, Forensic and Materials Sciences*, Springer International Publishing, 2022.
4 Y. Zhang, T. Zhang and H. Li, *Spectrochim. Acta, Part B*, 2021, **181**, 106218, DOI: 10.1016/j.sab.2021.106218.
5 S. Legnaioli, B. Campanella, F. Poggialini, S. Pagnotta, M. A. Harith, Z. A. Abdel-Salam and V. Palleschi, *Anal. Methods*, 2020, **12**, 1014–1029, DOI: 10.1039/C9AY02728A.
6 R. R. Hark and L. J. East, Forensic Applications of LIBS, in *Laser-Induced Breakdown Spectroscopy*, ed. S. Musazzi and U. Perini, Springer, Berlin, Heidelberg, 2014, pp. 377–420, DOI: 10.1007/978-3-642-45085-3_14.
7 F. Ruan, T. Zhang and H. Li, *Appl. Spectrosc. Rev.*, 2019, **54**, 573–601, DOI: 10.1080/05704928.2018.1491857.
8 J. Ren, Y. Zhao and K. Yu, *Computers and Electronics in Agriculture*, 2022, **197**, 106986, DOI: 10.1016/j.compag.2022.106986.
9 L. Brunnbauer, Z. Gajarska, H. Lohninger and A. Limbeck, *Trends Anal. Chem.*, 2023, **159**, 116859, DOI: 10.1016/j.trac.2022.116859.
10 M. Bucková, J. Hegrová, V. Jandová, J. Svodoba and R. Ličbinský, *J. Appl. Phycol.*, 2022, **34**, 2735–2742, DOI: 10.1007/s10811-022-02723-0.
11 A. Hrdlička, J. Hegrová, M. Bucková, D. Prochazka, M. Holá, K. Novotný, P. Pořízka, V. Kanický and J. Kaiser, *Spectrochim. Acta, Part B*, 2022, **195**, 106488, DOI: 10.1016/j.sab.2022.106488.
12 M. Garcimuño, D. M. Díaz Pace and G. Bertuccelli, *Opt. Laser Technol.*, 2013, **47**, 26–30, DOI: 10.1016/j.optlastec.2012.08.011.
13 J. Horská, A. Hrdlička, J. Hegrová, M. Bucková, D. Prochazka, P. Pořízka, V. Kanický and J. Kaiser, *Spectrochim. Acta, Part B*, 2024, **213**, 106883, DOI: 10.1016/j.sab.2024.106883.
14 B. T. Manard, S. E. Szakas, J. S. Stanberry, B. W. Ticknor, L. O'Brien, M. Boris, J. T. Hewitt, P. Cable-Dunlap and H. B. Andrews, *J. Anal. At. Spectrom.*, 2025, **40**, 1241–1248, DOI: 10.1039/d5ja00009b.
15 V. K. Singh, N. Sharma, O. N. Verma, V. K. Singh, D. K. Tripathi, Y. Lee, S. Kumar, P. K. Rai and M. A. Gondal, *At. Spectrosc.*, 2021, **42**, 99–113, DOI: 10.46770/AS.2020.201.
16 P. Pořízka, D. Prochazka, Z. Pilát, L. Krajcarová, J. Kaiser, R. Malina, J. Novotný, P. Zemánek, J. Ježek, M. Šerý, S. Bernatová, V. Krzyžánek, K. Dobranská, K. Novotný, M. Trtílek and O. Samek, *Spectrochim. Acta, Part B*, 2012, **74–75**, 169–176, DOI: 10.1016/j.sab.2012.06.014.
17 P. Pořízka, P. Prochazková, D. Prochazka, L. Sládková, J. Novotný, M. Petrilak, M. Brada, O. Samek, Z. Pilát, P. Zemánek, V. Adam, R. Kizek, K. Novotný and J. Kaiser, *Sensors*, 2014, **14**, 17725–17752, DOI: 10.3390/s140917725.
18 R. M. Alharbi, *Int. J. Pharm. Res. Allied Sci.*, 2017, **6**, 290–300.
19 K. Tsuyuki, S. Miura, N. Idris, K. H. Kurniawan, T. J. Lie and K. Kagawa, *Appl. Spectrosc.*, 2006, **60**, 61–64, DOI: 10.1366/000370206775382668.
20 G. S. Settles and M. J. Hargather, *Meas. Sci. Technol.*, 2017, **28**, 042001, DOI: 10.1088/1361-6501/aa5748.
21 J. Koch, S. Heiroth, T. Lippert and D. Günther, *Spectrochim. Acta, Part B*, 2010, **65**, 943–949, DOI: 10.1016/j.sab.2010.09.004.
22 J. Buday, P. Pořízka, M. Buchtová and J. Kaiser, *Spectrochim. Acta, Part B*, 2021, **182**, 106254, DOI: 10.1016/j.sab.2021.106254.
23 J. Buday, D. Prochazka, A. Záděra, V. Kaňa, P. Pořízka and J. Kaiser, *Spectrochim. Acta, Part B*, 2022, **194**, 106476, DOI: 10.1016/j.sab.2022.106476.
24 F. Rezaei and S. H. Tavassoli, *J. Anal. At. Spectrom.*, 2014, **29**, 2371–2378, DOI: 10.1039/C4JA00237G.
25 C. Gottlieb, A. Gojani, T. Völker, T. Günther, I. Gornushkin, G. Wilsch and J. Günster, *Spectrochim. Acta, Part B*, 2020, **165**, 105772, DOI: 10.1016/j.sab.2020.105772.
26 J. He and J. P. Chen, *Bioresour. Technol.*, 2014, **160**, 67–78, DOI: 10.1016/j.biortech.2014.01.068.
27 R. W. Dean and W. J. Dixon, *Anal. Chem.*, 1951, **23**, 636–638, DOI: 10.1021/ac60052a025.
28 X. Feng, Z. Jin, F. Meng, R. Liu, Y. Hou, H. Zhu and L. Wang, *J. Mater. Chem. C*, 2024, **12**, 18009, DOI: 10.1039/d4tc02544j.
29 G. Cristoforetti, A. De Giacomo, M. Dell'Aglio, S. Legnaioli, E. Tognoni, V. Palleschi and N. Omenetto, *Spectrochim. Acta, Part B*, 2010, **65**, 86–95, DOI: 10.1016/j.sab.2009.11.005.
30 https://physics.nist.gov/PhysRefData/ASD/levels_form.html, 4 November 2024.